Investigation of ρ-meson production in πp interactions at 3.9 GeV/c*

B. Haber,† M. F. Hodous, R. I. Hulsizer, V. Kistiakowsky, A. Levy,‡ I. A. Pless, R. A. Singer,§ J. Wolfson, and R. K. Yamamoto
Laboratory for Nuclear Science, Massachusetts Institute of Technology, Cambridge, Massachusetts 02139
(Received 6 February 1974)

We have investigated the ρ-meson production mechanism in the three reactions $\pi^+p \to \rho^+p$ and $\pi^-p \to \rho^0n$ at 3.9 GeV/c ($s = 8.2$ GeV^2) using the prism-plot technique. Differential cross sections at all momentum transfers are presented. A significant backward peak has been found in all three reactions. The differential cross sections for these backward peaks are given and are compared with the equivalent pion elastic and charge-exchange cross sections in the backward direction. Using a linear combination of the three differential cross sections we have isolated the $I = 0$ exchange contribution in the forward direction. This differential cross section has a zero at $-t = 0.45$ (GeV/c)^2 and is fitted by the dual absorptive model of Harari with an interaction radius of ~1.2 F. The total $I=0$ cross section is calculated and compared with similarly determined cross sections at higher momenta. An analysis of the properties of the other possible spin-parity exchanges is also presented.

I. INTRODUCTION

In this paper we present the results of an analysis of the three interactions

$$\pi^+p \to \rho^+p, \tag{1}$$

$$\pi^-p \to \rho^-p, \tag{2}$$

$$\pi^-p \to \rho^0n \tag{3}$$

at an incident momentum of 3.9 GeV/c ($s = 8.2$ GeV^2). The events are from a 600 000 picture exposure in the Argonne National Laboratory 30-in. hydrogen bubble chamber. The interactions were measured on the PEPR (precision encoding and pattern recognition) automatic measuring system at MIT and the three-body final states discussed here were analyzed using the three-body prism-plot technique.[1,2]

The simultaneous investigation of these three interactions has been of particular interest since it was pointed out by Contogouris, Tran Thanh Van, and Lubatti[3] that a linear combination of the three differential cross sections allows the separation of the $I = 0$ exchange contribution in the t channel. Since there is only one known meson with the proper quantum numbers this is usually identified as ω exchange. This possibility of isolating a contribution involving only the exchange of a single resonance (or Regge trajectory) allows tests of theoretical models in the cleanest possible way. In particular we have compared the dual absorptive model of Harari[4] with our data and with the results of the same analysis applied to other data at 6 GeV/c ($s = 12.2$ GeV^2) (see Ref. 5) and 16 GeV/c ($s = 31$ GeV^2) (see Ref. 6).

In Sec. II we discuss the data collection and the separation into the three final states (1)–(3). In Sec. III we present the total and differential cross sections for the production of ρ mesons and the density matrix elements determined for their decay. Because of the use of the prism-plot technique these cross sections could be determined at all momentum transfers and a significant backward peak has been found. The differential cross section for this backward production is presented and compared with pion backward elastic and charge-exchange scattering. In Sec. IV the $I = 0$ exchange contribution is isolated and compared with the models of Harari and Schwimmer.[7] The energy dependence of this cross section is examined using the 6-GeV/c and 16-GeV/c data. Section V contains a brief discussion of the separation of the pion exchange component. In the last section we summarize our results.

II. DATA ANALYSIS

All interactions found in the film were digitized. Approximately 70% of the interactions were measured on PEPR and the remaining events on film plane digitizers. This analysis is based upon 27 000 two prong events in the π^+ exposure and 24 000 events in the π^- exposure. All of the events were processed through the Maryland version of TVGP and SQUAW. The details of the criteria by which events were assigned to a particular final state are given elsewhere.[8]

The number of events found in each of the three final states used in this analysis and their cross sections are given in Table I. A detailed study of the missing-mass distribution indicates that the contamination of the one-constraint (1C) final

states by the multiple neutral final states is less than 5%. The errors which are quoted in this paper are purely statistical.

In Figs. 1–3 we show the two-body invariant mass plots for each of the three final states. There are clearly large signals for all three charge states of the ρ meson, although in each case there is also a sizable background under the peak. In order to obtain a pure sample of events without making mass cuts or background subtractions, which might bias the data, each of these final states has been analyzed using the three-body prism-plot technique developed at MIT. Details of this method have been described previously[1,2] and will not be discussed here. The most important feature of this technique is that it uses all $(3N-5)$ independent kinematic variables necessary to specify an N-particle final state. Extensive Monte Carlo tests of this method have been carried out and indicate that there is less than a 5% misidentification of events.

In Fig. 4 we show the dipion invariant mass distribution for each of the three channels. The events have been weighted by the probability that they form a ρ meson as determined by the prism-plot technique. Each of these distributions has been fitted to a modified Breit-Wigner shape of the form

$$\frac{M}{q}\,\frac{\Gamma^2}{(M^2-M_0^2)^2+M_0^2\Gamma^2}\,,\quad \Gamma=\Gamma_0\left(\frac{q}{q_0}\right)^{2l+1} \tag{4}$$

where M_0 and Γ_0 are the fitted values for the mass and width of the resonance, q_0 and q are the momenta for the decays of the particles of mass M_0 and M, respectively, and l is the orbital angular momentum of the resonance, which is 1 for the ρ meson. The results of the fit for the three charged states of the ρ meson are given in Table II. It should be emphasized that there is no background term in these fits, indicating that the sample is very clean, and that there is no need for mass cuts or background subtractions. We have examined these events carefully and find no biases

TABLE I. Event samples and cross sections.

Final state	Events	Cross section (mb)
$p\pi^+\pi^0$	3095	2.30 ± 0.06
$p\pi^-\pi^0$	2579	2.08 ± 0.07
$n\pi^+\pi^-$	3441	2.75 ± 0.08

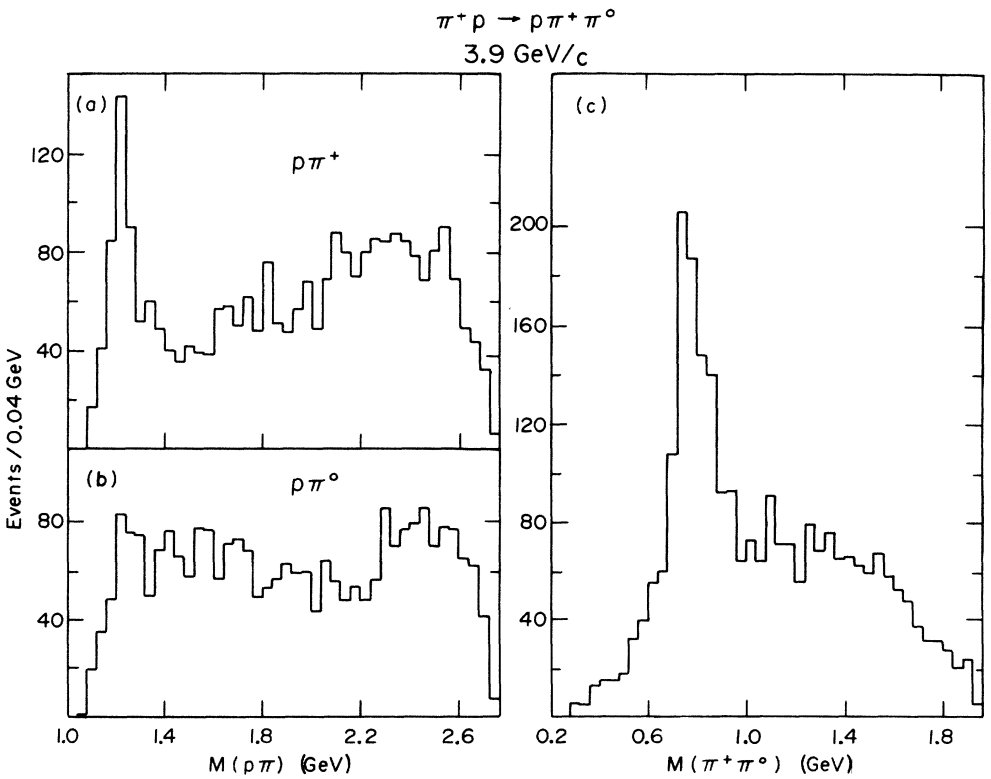

FIG. 1. Two-body invariant masses for the reaction $\pi^+p\to p\pi^+\pi^0$: (a) $M(p\pi^+)$, (b) $M(p\pi^0)$, and (c) $M(\pi^+\pi^0)$.

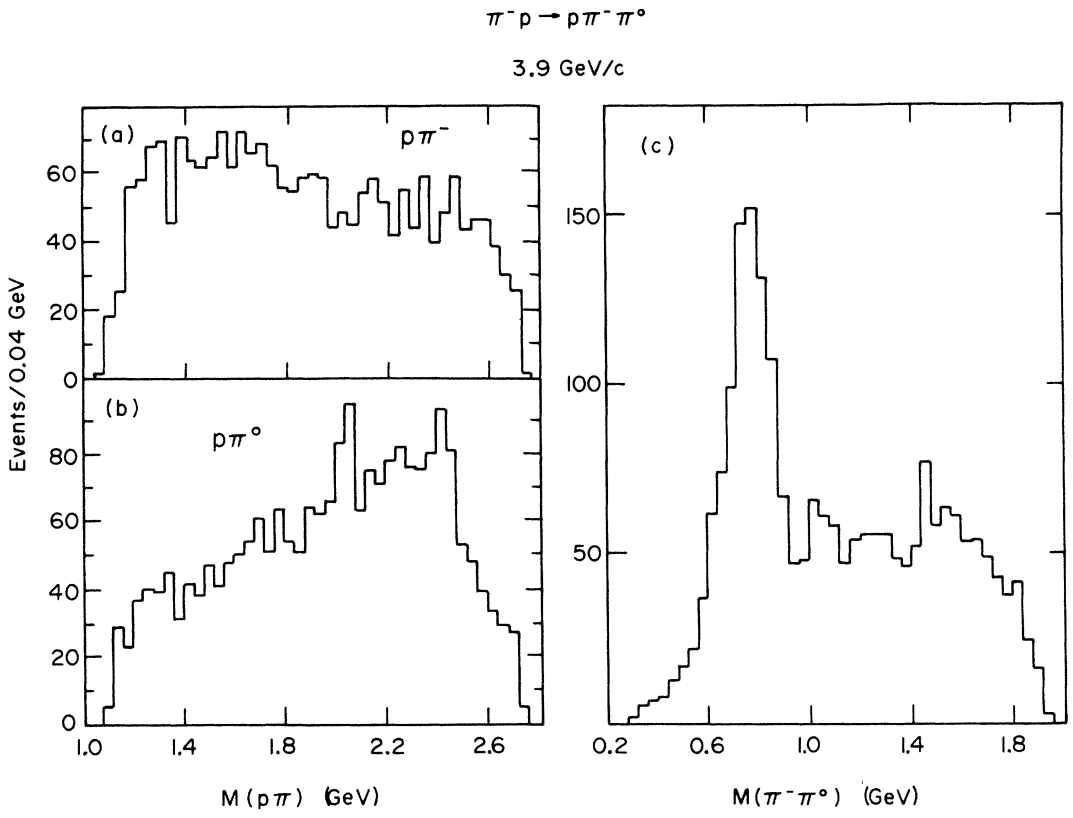

FIG. 2. Two-body invariant masses for the reaction $\pi^- p \to p\pi^-\pi^0$: (a) $M(p\pi^-)$, (b) $M(p\pi^0)$, and (c) $M(\pi^-\pi^0)$.

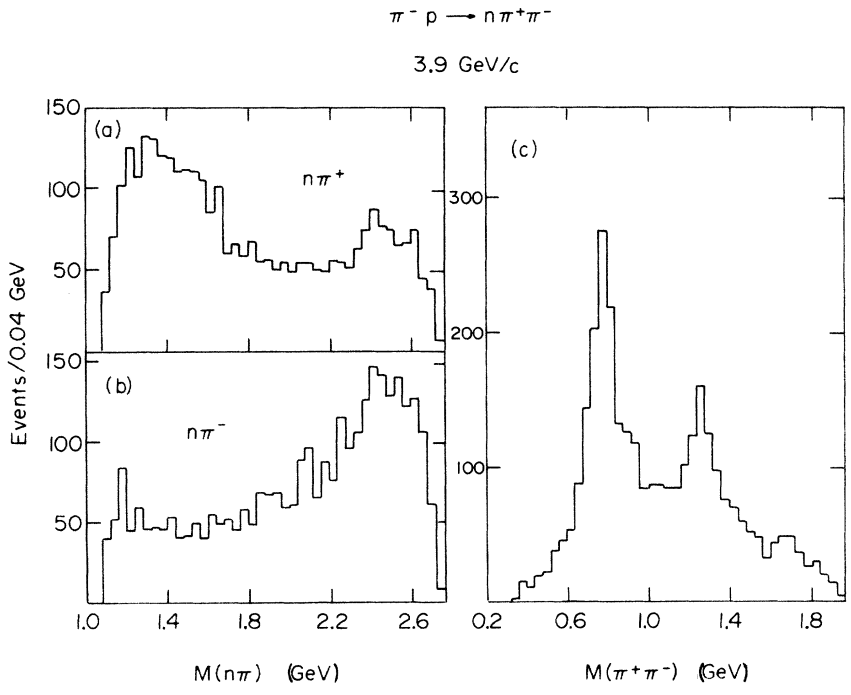

FIG. 3. Two-body invariant masses for the reaction $\pi^- p \to n\pi^+\pi^-$: (a) $M(n\pi^+)$, (b) $M(n\pi^-)$, and (c) $M(\pi^+\pi^-)$.

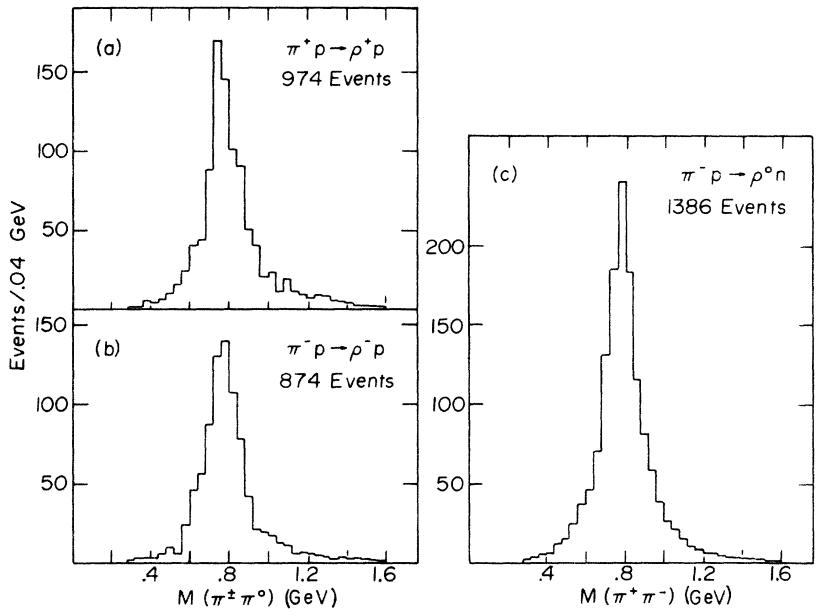

FIG. 4. Dipion mass distributions for events chosen as ρ events by the prism plot technique (see text) for the reactions: (a) $\pi^+ p \to \rho^+ p$, (b) $\pi^- p \to \rho^- p$, and (c) $\pi^- p \to \rho^0 n$.

in the data as a function of either mass or momentum transfer.

III. DIFFERENTIAL CROSS SECTIONS AND DENSITY MATRIX ELEMENTS

The differential cross sections for the three interactions are shown in Fig. 5 and listed in Table III. The charged-ρ distributions are very similar, showing an exponential fall at small values of t, a dip at $|t| \sim 0.45$ (GeV/c)^2, a second minimum at $|t| \sim 3$ (GeV/c)^2, and a broad backward peak. The measurement at the lowest value of t is biased due to scanning and measuring loss for low-momentum recoil protons. Based upon our analysis of the loss of events at small t in the elastic channels,[8] we can estimate a correction to the cross section in this first bin which yields an approximate value consistent with the exponential behavior of the rest of the data [$t_{\min}$ for this reaction is -0.01 (GeV/c)^2]. The neutral ρ also shows an exponential drop for small values of $|t|$; however, there is no dip at 0.45 (GeV/c)^2, although the slope appears to change in that region. There is a dip at ~3 (GeV/c)^2 and a broad backward peak similar to the charged-ρ distribution.

A. Forward production and decay

The small-t regions have been fitted to the form Ae^{bt}. The momentum transfer range used is $0.05 \leq |t| \leq 0.3$ (GeV/c)^2. The results of these fits and the total cross section for each of the channels (integrated over all t) are given in Table IV.

The density matrix elements have been determined as functions of momentum transfer in both the Gottfried-Jackson frame[9] (t channel) and the helicity frame (s channel). These elements have been evaluated by fitting the function $W(\theta,\phi)$ to the angular distributions in these reference frames, where

$$W(\theta,\phi) = \frac{3}{4\pi}\left[\frac{\sin^2\theta}{2} + \left(\frac{3\cos^2\theta - 1}{2}\right)\left(\rho_{00} + \frac{\rho_{ss}}{3}\right) - \rho_{1-1}\sin^2\theta\cos 2\phi - \sqrt{2}\,\mathrm{Re}\rho_{10}\sin 2\theta\cos\phi + \frac{2}{\sqrt{3}}\mathrm{Re}\rho_{s0}\cos\theta - \frac{2\sqrt{2}}{\sqrt{3}}\mathrm{Re}\rho_{s1}\sin\theta\cos\phi\right]. \quad (5)$$

The subscript s is used to distinguish the s-wave component present in the ρ^0 decay. For the $\rho^\pm$ only the p-wave terms were used in the fit. It is clearly not possible to determine the values of ρ_{00} and ρ_{ss} separately in the case where there is an s-wave interference term. For the remainder of the analysis we have "absorbed" the ρ_{ss} term into

TABLE II. Mass and width for the ρ meson.

	M_0 (MeV)	Γ_0 (MeV)
ρ^+	772±4	164±10
ρ^-	767±3	156±8
ρ^0	783±3	172±8

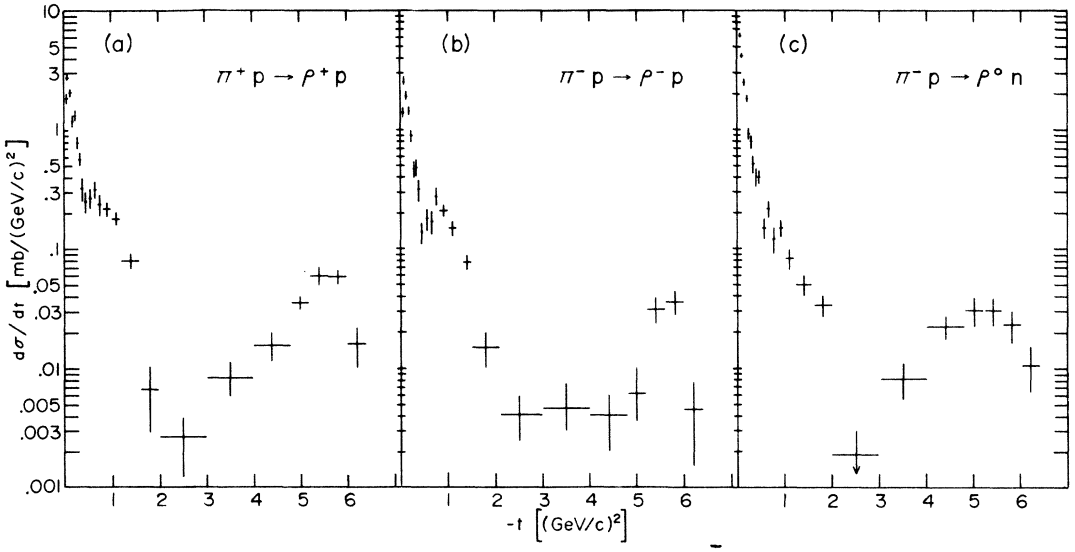

FIG. 5. The differential cross sections for (a) $\pi^+ p \to \rho^+ p$, (b) $\pi^- p \to \rho^- p$, and (c) $\pi^- p \to \rho^0 n$.

ρ_{00}. At 6 GeV/c the positivity requirements on the matrix element have been used to determine that ρ_{ss} is relatively small, in the range of 0.1 to 0.2.[5] No such upper limit can be determined from our data.

The matrix elements have been determined by the method of moments using the following relations:

$$\rho_{00} = \tfrac{1}{2}(5\langle\cos^2\theta\rangle - 1), \tag{6}$$

$$\rho_{1-1} = -\tfrac{5}{4}\langle\sin^2\theta\cos 2\phi\rangle, \tag{7}$$

$$\mathrm{Re}\rho_{10} = -\tfrac{5}{4}\sqrt{2}\,\langle\sin 2\theta\cos\phi\rangle, \tag{8}$$

$$\mathrm{Re}\rho_{s0} = (\tfrac{3}{8})^{1/2}\langle\cos\theta\rangle, \tag{9}$$

$$\mathrm{Re}\rho_{s1} = -(\tfrac{3}{8})^{1/2}\langle\sin\theta\cos\phi\rangle. \tag{10}$$

Both reference frames are defined by first transforming all particles into the rest frame of the resonance. In the Gottfried-Jackson frame the z axis is defined as the direction of the incident pion as seen in that frame, while for the helicity frame this axis is taken as the negative of the direction of the nucleon in the final state.

Figures 6–8 and Tables V–VII show the density matrix for the three final states. The shapes of the ρ^+ and ρ^- matrix elements are very similar to each other but different from those of the ρ^0. For ρ^0 production, the value of $\mathrm{Re}\rho_{s0}$ is the measure of the forward-backward asymmetry of its decay and shows the t dependence which has been previously observed.[5,6] The most prominent feature

TABLE III. Differential cross sections for $\pi^\pm p \to \rho N$.

$\lvert t\rvert$ [(GeV/c)^2]	$\frac{d\sigma}{dt}$ [mb/(GeV/c)^2] $\pi^+ p \to \rho^+ p$	$\pi^- p \to \rho^- p$	$\pi^- p \to \rho^0 n$
0.00–0.05	1.81 ± 0.18	1.43 ± 0.15	6.30 ± 0.32
0.05–0.10	2.77 ± 0.22	2.57 ± 0.20	4.19 ± 0.26
0.10–0.15	2.06 ± 0.19	1.97 ± 0.18	2.51 ± 0.20
0.15–0.20	1.19 ± 0.14	1.46 ± 0.15	1.86 ± 0.17
0.20–0.25	1.36 ± 0.16	0.88 ± 0.12	0.94 ± 0.12
0.25–0.30	0.82 ± 0.12	0.47 ± 0.09	0.79 ± 0.11
0.30–0.35	0.57 ± 0.10	0.49 ± 0.09	0.53 ± 0.09
0.35–0.40	0.33 ± 0.08	0.32 ± 0.07	0.40 ± 0.08
0.40–0.50	0.25 ± 0.05	0.14 ± 0.03	0.40 ± 0.06
0.50–0.60	0.27 ± 0.05	0.18 ± 0.04	0.15 ± 0.03
0.60–0.70	0.32 ± 0.05	0.17 ± 0.04	0.22 ± 0.04
0.70–0.80	0.24 ± 0.05	0.28 ± 0.05	0.12 ± 0.03
0.80–1.00	0.22 ± 0.031	0.21 ± 0.029	0.15 ± 0.024
1.00–1.20	0.18 ± 0.028	0.15 ± 0.025	0.083 ± 0.018
1.20–1.60	0.080 ± 0.013	0.078 ± 0.012	0.050 ± 0.010
1.60–2.00	0.007 ± 0.004	0.015 ± 0.005	0.034 ± 0.008
2.00–3.00	0.003 ± 0.001	0.004 ± 0.002	0.002 ± 0.001
3.00–4.00	0.009 ± 0.003	0.005 ± 0.002	0.008 ± 0.003
4.00–4.80	0.016 ± 0.004	0.004 ± 0.002	0.022 ± 0.005
4.80–5.20	0.040 ± 0.010	0.006 ± 0.004	0.030 ± 0.008
5.20–5.60	0.059 ± 0.012	0.031 ± 0.008	0.030 ± 0.008
5.60–6.00	0.058 ± 0.011	0.036 ± 0.008	0.023 ± 0.007
6.00–6.40	0.016 ± 0.006	0.004 ± 0.003	0.010 ± 0.005

TABLE IV. Total cross section for ρ-meson production and the forward slope of the differential cross-section fit to the form Ae^{bt}.

	b [(GeV/c)$^{-2}$]	σ_{tot} (mb)
ρ^+	6.0 ± 1.1	0.86 ± 0.03
ρ^-	7.7 ± 0.8	0.70 ± 0.02
ρ^0	8.9 ± 0.7	1.11 ± 0.03

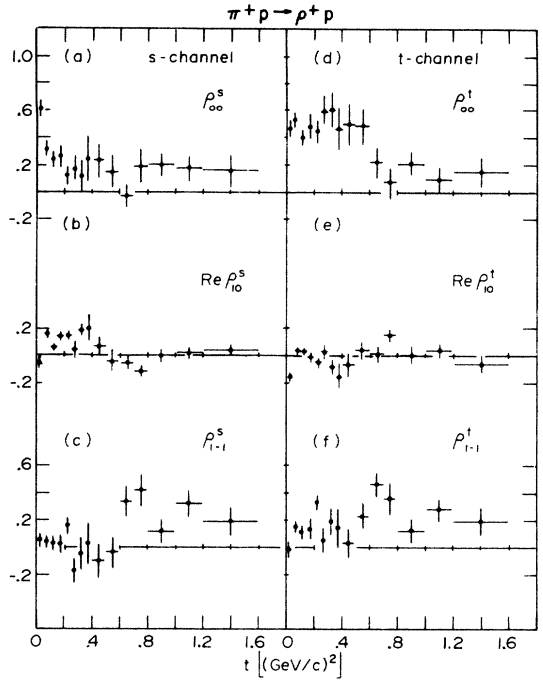

FIG. 6. The density matrix elements for the reaction $\pi^+p \to \rho^+p$.

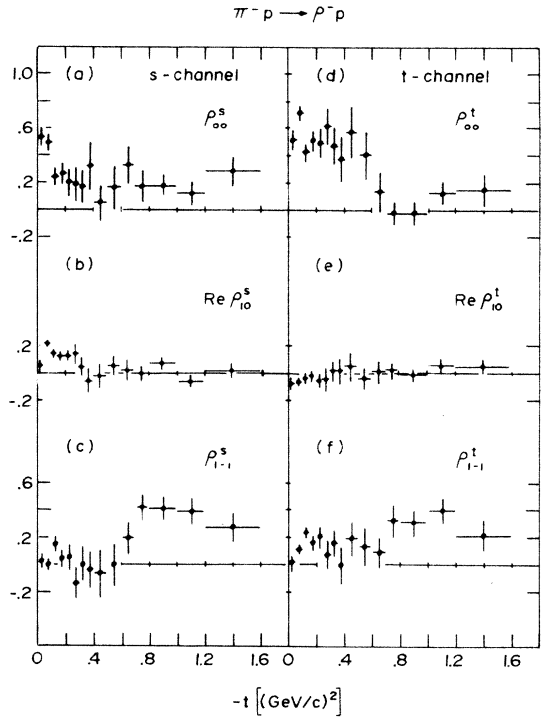

FIG. 7. The density matrix elements for the reaction $\pi^-p \to \rho^-p$.

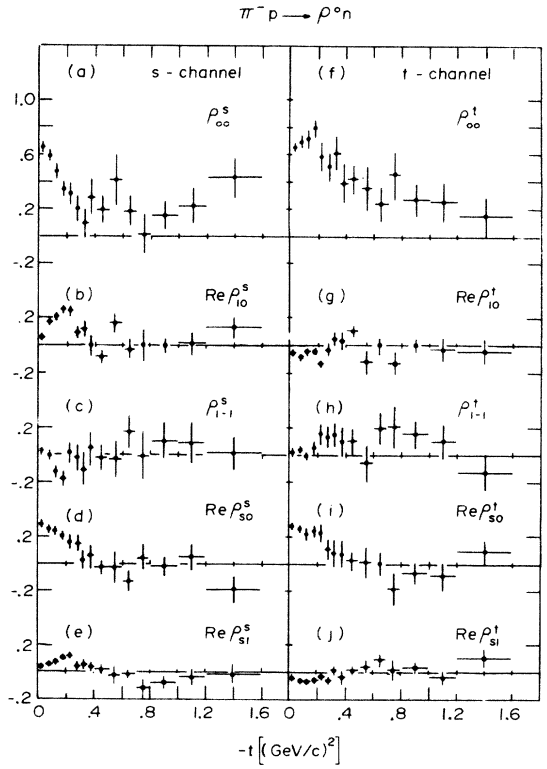

FIG. 8. The density matrix elements for the reaction $\pi^-p \to \rho^0n$.

of these distributions is the sharp drop in the value of ρ^t_{00} to ~0 for $\rho^\pm$ and to a minimum for the ρ^0 at a momentum transfer of ~0.6 $(\text{GeV}/c)^2$. This matrix element measures the amount of unnatural-parity exchange with no helicity flip in the t channel.[9]

It is also possible to select the natural- and unnatural-parity exchange contributions in the t channel when the meson does undergo a helicity flip by using the combination of matrix elements $\rho_{11}+\rho_{1-1}$ and $\rho_{11}-\rho_{1-1}$.[10] These matrix elements are shown in Fig. 9 and listed in Tables VIII–X. This separation is valid to the order of $1/s$ and only if there is no absorption present, since it would tend to mix amplitudes. If, however, elastic scattering conserves helicity in the s channel, then these relations are true in that frame even with absorption. The value of $\rho_{11}+\rho_{1-1}$ has no superscript because it is an invariant of the two reference frames considered.

The most distinctive feature in the case of both the ρ^+ and ρ^- productions is the sharp rise in the natural-parity contribution at momentum transfer values of ~0.6 $(\text{GeV}/c)^2$ with a corresponding drop in the unnatural exchange, particularly in the helicity-nonflip term (ρ_{00}) as mentioned above.

B. Backward production

Use of the prism-plot technique has allowed us to separate a clean sample of backward ρ-meson

TABLE V. Density matrix elements for $\pi^+ p \to \rho^+ p$.

$\lvert t\rvert$ [(GeV/c)^2]	s channel ρ_{00}	s channel Reρ_{10}	s channel ρ_{1-1}	t channel ρ_{00}	t channel Reρ_{10}	t channel ρ_{1-1}
0.00–0.05	0.61±0.07	−0.05±0.05	0.05±0.05	0.47±0.07	−0.16±0.05	−0.02±0.06
0.05–0.10	0.31±0.06	0.17±0.03	0.04±0.05	0.54±0.06	0.04±0.04	0.15±0.05
0.10–0.15	0.24±0.06	0.06±0.04	0.03±0.06	0.40±0.07	0.03±0.04	0.11±0.05
0.15–0.20	0.26±0.09	0.14±0.05	0.02±0.08	0.49±0.10	−0.02±0.05	0.13±0.08
0.20–0.25	0.12±0.07	0.15±0.04	0.16±0.08	0.45±0.09	−0.05±0.04	0.32±0.06
0.25–0.30	0.16±0.10	0.05±0.07	−0.17±0.10	0.60±0.12	0.03±0.07	0.05±0.08
0.30–0.35	0.12±0.12	0.19±0.06	−0.05±0.12	0.60±0.14	−0.08±0.07	0.19±0.10
0.35–0.40	0.25±0.16	0.10±0.11	0.03±0.16	0.46±0.17	−0.15±0.11	0.14±0.15
0.40–0.50	0.23±0.13	0.07±0.09	−0.10±0.13	0.50±0.16	−0.07±0.09	0.03±0.11
0.50–0.60	0.15±0.12	−0.04±0.08	−0.04±0.12	0.49±0.14	0.04±0.08	0.13±0.10
0.60–0.70	−0.03±0.09	−0.05±0.06	0.34±0.11	0.22±0.12	0.01±0.06	0.46±0.09
0.70–0.80	0.19±0.13	−0.11±0.06	0.42±0.12	0.07±0.12	0.14±0.07	0.36±0.12
0.80–1.00	0.20±0.09	0.00±0.06	0.12±0.09	0.21±0.09	0.00±0.06	0.12±0.09
1.00–1.20	0.17±0.10	0.02±0.06	0.32±0.10	0.09±0.10	0.02±0.06	0.28±0.09
1.20–1.60	0.16±0.10	0.04±0.06	0.19±0.10	0.15±0.11	−0.06±0.06	0.18±0.10

production. Figure 5 shows these backward peaks for the three reactions. The maximum momentum transfer kinematically allowed for a beam momentum of 3.9 GeV/c and a ρ mass of 0.76 GeV is 6.0 (GeV/c)^2. The events at $|t| > 6.0$ (GeV/c)^2 are the result of the spread in beam momentum and the width of the ρ meson. The drop in cross section in that region is not, therefore, physically significant.

In Fig. 10 we show the invariant mass distributions for the ρ-meson events produced in the backward hemisphere. The total number of events and their cross section is given in Table XI.

Our backward ρ^0 cross section agrees quite well with the value of 87±15 μb found in a $\pi^- p$ experiment at 4 GeV/c.[11] In that experiment they estimate a ρ^- cross section of 18±5 μb which is somewhat lower than what we find. Our backward ρ^+ cross section is considerably larger than the 20–25 μb found in a $\pi^+ p$ experiment at 4 GeV/c,[12] just as our total cross section for ρ^+ production reported previously[8] is much greater than theirs.

In Fig. 11 and Table XII we show the differential cross sections for the three reactions as a function of momentum transfer in the cross channel (u channel) for $-0.03 < -u < 2.0$ (GeV/c)^2. As a comparison we also show the shape of the backward cross section for the elastic $\pi^\pm p \to \pi^\pm p$ interactions and the charge-exchange interaction $\pi^- p \to \pi^0 n$. In order to determine these shapes we have examined the available data on these interactions for incident pion momenta between 3.5 and 4.3 (GeV/c).[13] Although the relative normalization differs between several of the experiments, the general shapes of

TABLE VI. Density matrix elements for $\pi^- p \to \rho^- p$.

$\lvert t\rvert$ [(GeV/c)^2]	s channel ρ_{00}	s channel Reρ_{10}	s channel ρ_{1-1}	t channel ρ_{00}	t channel Reρ_{10}	t channel ρ_{1-1}
0.00–0.05	0.53±0.07	0.05±0.06	0.02±0.06	0.51±0.08	−0.07±0.05	0.01±0.06
0.05–0.10	0.49±0.06	0.22±0.04	0.00±0.05	0.71±0.06	−0.06±0.04	0.11±0.04
0.10–0.15	0.24±0.07	0.14±0.04	0.14±0.06	0.42±0.07	−0.03±0.04	0.23±0.05
0.15–0.20	0.26±0.08	0.12±0.04	0.04±0.07	0.50±0.08	−0.02±0.05	0.16±0.06
0.20–0.25	0.20±0.10	0.13±0.05	0.05±0.10	0.49±0.11	−0.05±0.06	0.20±0.08
0.25–0.30	0.19±0.13	0.14±0.09	−0.14±0.12	0.61±0.14	−0.04±0.09	0.07±0.11
0.30–0.35	0.17±0.12	0.05±0.08	0.00±0.13	0.47±0.14	0.02±0.08	0.16±0.10
0.35–0.40	0.32±0.18	−0.05±0.09	−0.04±0.14	0.37±0.17	0.02±0.10	−0.01±0.14
0.40–0.50	0.05±0.13	−0.02±0.11	−0.07±0.18	0.56±0.20	0.04±0.11	0.19±0.13
0.50–0.60	0.16±0.16	0.05±0.09	0.01±0.16	0.40±0.18	−0.04±0.08	0.13±0.14
0.60–0.70	0.33±0.14	0.02±0.08	0.19±0.13	0.13±0.15	0.01±0.09	0.09±0.11
0.70–0.80	0.17±0.12	−0.01±0.06	0.42±0.10	−0.03±0.09	0.02±0.06	0.32±0.12
0.80–1.00	0.17±0.09	0.07±0.05	0.41±0.09	−0.03±0.09	−0.01±0.05	0.30±0.10
1.00–1.20	0.12±0.10	−0.06±0.06	0.39±0.10	0.12±0.09	0.06±0.06	0.39±0.10
1.20–1.60	0.28±0.11	0.02±0.07	0.27±0.10	0.14±0.12	0.05±0.06	0.21±0.11

the differential cross sections are similar. It is an average of these shapes, with arbitrary normalizations, which are shown in Fig. 11.

Good agreement is found for the charge-exchange reaction [Fig. 11(c)]. The dip at $-u \sim 0.2$ (GeV/c)^2 is predicted, using a simple Regge-pole model, due to a wrong-signature nonsense zero (WSNZ) of the N_α trajectory at this value. Within the limited statistics for the ρ^- production, our data are also consistent with the π^- elastic scattering [Fig. 11(b)].

The ρ^+ data [Fig. 11(a)], however, are definitely in disagreement with the corresponding $\pi^+ p$ backward elastic scattering. Although we see evidence for a dip at $-u \sim 0.2$ (GeV/c)^2 the decrease in cross section beyond that dip is much steeper than the elastic scattering. This trend has also been seen in other experiments at 5.0 and 5.2 GeV/c (see Refs. 14 and 15, respectively) which investigated backward ρ^+ production. These experiments found an exponential decrease of the form Ae^{bu} with values for b of 1.7 ± 0.06 and 2.9 ± 0.6 (GeV/c)$^{-2}$, respectively. They do not, however, see any evidence for a dip at $-u \sim 0.2$ (GeV/c)^2 although again it is expected from the WSNZ of the N_α trajectory. If we fit our data out to $-u = 0.8$ (GeV/c)^2 to the exponential form, we get an acceptable fit (30% probability) with a slope of 2.4 ± 0.6 (GeV/c)$^{-2}$. Hence these data are consistent with the previous work and highlight the question of the similarity of the ρ^- and ρ^0 distributions with the elastic cross sections and the disagreement of the ρ^+ production with these cross sections.

IV. $I=0$ EXCHANGE

It is possible using these three reactions to isolate the contribution of $I=0$ and $I=1$ t-channel exchanges to the ρ-meson production. If I_0 and I_1 represent the amplitude for these two exchanges, then

$$\sigma_+ = |I_0 + I_1|^2, \tag{11}$$

$$\sigma_- = |I_0 - I_1|^2, \tag{12}$$

$$\sigma_0 = 2|I_1|^2, \tag{13}$$

where σ_+, σ_-, and σ_0 are the cross sections for ρ^+, ρ^-, and ρ^0 production, respectively. Solving these relations for the differential cross section for the $I=0$ exchange contribution gives

$$\left.\frac{d\sigma}{dt}\right|_{I=0} = \frac{1}{2}\left(\frac{d\sigma_+}{dt} + \frac{d\sigma_-}{dt} - \frac{d\sigma_0}{dt}\right). \tag{14}$$

TABLE VII. Density matrix elements for $\pi^- p \to \rho^0 n$.

$\lvert t\rvert$	s channel				t channel			
[(GeV/c)^2]	$\rho_{00}+\frac{1}{3}\rho_{ss}$	$\mathrm{Re}\rho_{10}$	ρ_{1-1}	$\mathrm{Re}\rho_{s0}$	$\mathrm{Re}\rho_{s1}$	$\rho_{00}+\frac{1}{3}\rho_{ss}$	$\mathrm{Re}\rho_{10}$	ρ_{1-1}	$\mathrm{Re}\rho_{s0}$	$\mathrm{Re}\rho_{s1}$
0.00–0.05	0.65 ± 0.04	0.08 ± 0.02	0.02 ± 0.03	0.28 ± 0.03	0.04 ± 0.02	0.65 ± 0.04	−0.06 ± 0.02	0.02 ± 0.03	0.28 ± 0.03	−0.04 ± 0.02
0.05–0.10	0.59 ± 0.05	0.17 ± 0.03	−0.01 ± 0.04	0.25 ± 0.03	0.06 ± 0.02	0.68 ± 0.05	−0.09 ± 0.03	0.04 ± 0.03	0.25 ± 0.03	−0.06 ± 0.02
0.10–0.15	0.47 ± 0.06	0.21 ± 0.04	−0.13 ± 0.05	0.24 ± 0.04	0.06 ± 0.03	0.71 ± 0.06	−0.05 ± 0.04	−0.01 ± 0.04	0.22 ± 0.04	−0.07 ± 0.02
0.15–0.20	0.33 ± 0.06	0.26 ± 0.04	−0.18 ± 0.06	0.20 ± 0.04	0.11 ± 0.03	0.78 ± 0.07	−0.05 ± 0.04	0.05 ± 0.04	0.24 ± 0.05	−0.06 ± 0.03
0.20–0.25	0.31 ± 0.09	0.24 ± 0.05	0.01 ± 0.08	0.16 ± 0.06	0.12 ± 0.04	0.59 ± 0.10	−0.13 ± 0.05	0.14 ± 0.07	0.23 ± 0.07	−0.04 ± 0.04
0.25–0.30	0.20 ± 0.10	0.09 ± 0.06	−0.02 ± 0.10	0.15 ± 0.06	0.04 ± 0.05	0.51 ± 0.11	−0.03 ± 0.06	0.13 ± 0.08	0.11 ± 0.08	−0.07 ± 0.04
0.30–0.35	0.09 ± 0.11	0.12 ± 0.08	−0.11 ± 0.12	0.03 ± 0.07	0.05 ± 0.07	0.61 ± 0.13	0.03 ± 0.08	0.15 ± 0.09	0.08 ± 0.10	0.01 ± 0.05
0.35–0.40	0.28 ± 0.14	0.00 ± 0.09	0.04 ± 0.13	0.06 ± 0.10	0.04 ± 0.07	0.39 ± 0.15	0.04 ± 0.09	0.10 ± 0.11	0.07 ± 0.10	−0.03 ± 0.06
0.40–0.50	0.19 ± 0.11	−0.08 ± 0.06	−0.02 ± 0.10	−0.02 ± 0.06	0.02 ± 0.05	0.42 ± 0.11	0.11 ± 0.06	0.10 ± 0.10	0.02 ± 0.07	0.01 ± 0.04
0.50–0.60	0.41 ± 0.19	0.16 ± 0.09	−0.03 ± 0.14	−0.03 ± 0.12	−0.02 ± 0.08	0.35 ± 0.17	−0.12 ± 0.11	−0.06 ± 0.14	0.01 ± 0.12	0.04 ± 0.08
0.60–0.70	0.18 ± 0.12	−0.02 ± 0.09	0.17 ± 0.12	−0.13 ± 0.08	−0.01 ± 0.06	0.24 ± 0.13	0.00 ± 0.08	0.20 ± 0.12	0.00 ± 0.09	0.10 ± 0.06
0.70–0.80	0.01 ± 0.15	0.00 ± 0.12	−0.01 ± 0.17	0.05 ± 0.10	−0.13 ± 0.09	0.45 ± 0.17	−0.12 ± 0.11	0.21 ± 0.16	−0.19 ± 0.13	0.01 ± 0.08
0.80–1.00	0.15 ± 0.11	−0.01 ± 0.06	0.10 ± 0.12	−0.02 ± 0.07	−0.07 ± 0.06	0.27 ± 0.12	−0.01 ± 0.07	0.16 ± 0.10	−0.07 ± 0.08	0.03 ± 0.05
1.00–1.20	0.22 ± 0.13	0.01 ± 0.10	0.08 ± 0.14	0.05 ± 0.10	−0.03 ± 0.08	0.25 ± 0.15	−0.03 ± 0.10	0.10 ± 0.13	−0.09 ± 0.10	−0.02 ± 0.08
1.20–1.60	0.43 ± 0.15	0.13 ± 0.09	0.01 ± 0.12	−0.19 ± 0.10	0.00 ± 0.07	0.15 ± 0.12	−0.05 ± 0.10	−0.13 ± 0.13	0.09 ± 0.09	0.11 ± 0.08

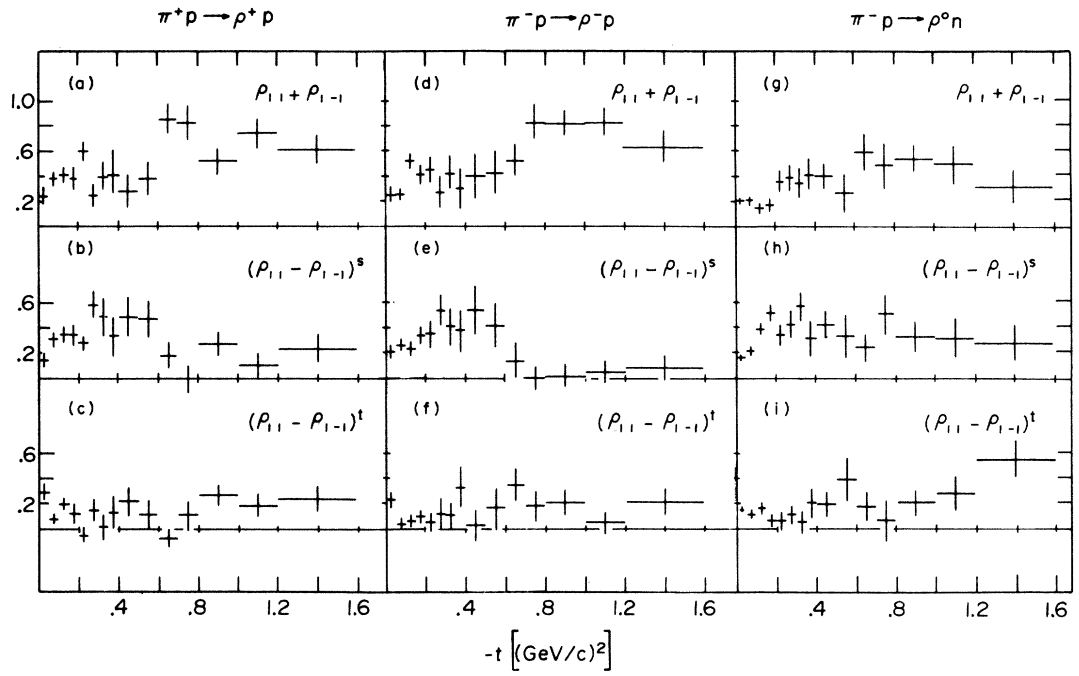

FIG. 9. The combined density matrix elements $\rho_{11}+\rho_{1-1}$ and $\rho_{11}-\rho_{1-1}$ for the three reactions: (a)–(c) $\pi^+p \to \rho^+p$, (d)–(f) $\pi^-p \to \rho^-p$, and (g)–(i) $\pi^-p \to \rho^0n$.

In Fig. 12(a) and Table XIII we show the cross section for this process along with the $I=1$ cross section derived directly from the ρ^0 differential cross section [relation (13)], for $0 \leq |t| \leq 1.6$ $(\mathrm{GeV}/c)^2$. The $I=1$ cross section falls smoothly out to the largest momentum transfer shown while the $I=0$ cross section has a zero at $|t| \sim 0.45$ $(\mathrm{GeV}/c)^2$ and then rises to a second maximum at $|t| \sim 1.0$ $(\mathrm{GeV}/c)^2$. The curve shown in Fig. 12(a) through the $I=1$ exchange data is a hand-drawn curve to guide the eye. The curve through the $I=0$ exchange data is from the dual absorptive model fit discussed below. The interference term, $\mathrm{Re}(I_0 I_1^*)$ is shown in Fig. 12(b) and is consistent with zero for all momentum transfer.

Figure 13 shows the $I=0$ exchange cross section in greater detail with a linear scale. The zero at 0.45 $(\mathrm{GeV}/c)^2$ corresponds to the first zero of the

TABLE VIII. $\rho_{11}+\rho_{1-1}$ and $\rho_{11}-\rho_{1-1}$ for $\pi^+p \to \rho^+p$.

$\lvert t\rvert$ $[(\mathrm{GeV}/c)^2]$	$\rho_{11}+\rho_{1-1}$	s channel $\rho_{11}-\rho_{1-1}$	t channel $\rho_{11}-\rho_{1-1}$
0.00–0.05	0.24±0.07	0.15±0.06	0.29±0.07
0.05–0.10	0.38±0.06	0.31±0.06	0.08±0.05
0.10–0.15	0.41±0.07	0.35±0.07	0.19±0.06
0.15–0.20	0.38±0.10	0.35±0.09	0.12±0.09
0.20–0.25	0.60±0.09	0.28±0.08	−0.05±0.06
0.25–0.30	0.25±0.10	0.59±0.11	0.15±0.10
0.30–0.35	0.39±0.13	0.49±0.14	0.01±0.11
0.35–0.40	0.41±0.20	0.34±0.17	0.13±0.14
0.40–0.50	0.28±0.14	0.49±0.16	0.22±0.12
0.50–0.60	0.38±0.14	0.47±0.14	0.12±0.11
0.60–0.70	0.85±0.13	0.18±0.11	−0.07±0.08
0.70–0.08	0.82±0.15	−0.01±0.12	0.11±0.12
0.80–1.00	0.52±0.11	0.28±0.10	0.27±0.09
1.00–1.20	0.73±0.12	0.10±0.10	0.18±0.10
1.20–1.60	0.61±0.12	0.24±0.12	0.24±0.11

TABLE IX. $\rho_{11}+\rho_{1-1}$ and $\rho_{11}-\rho_{1-1}$ for $\pi^-p \to \rho^-p$.

$\lvert t\rvert$ $[(\mathrm{GeV}/c)^2]$	$\rho_{11}+\rho_{1-1}$	s channel $\rho_{11}-\rho_{1-1}$	t channel $\rho_{11}-\rho_{1-1}$
0.00–0.05	0.25±0.07	0.21±0.06	0.23±0.07
0.05–0.10	0.25±0.06	0.26±0.05	0.04±0.05
0.10–0.15	0.52±0.07	0.23±0.06	0.06±0.05
0.15–0.20	0.41±0.08	0.33±0.08	0.10±0.06
0.20–0.25	0.45±0.11	0.35±0.11	0.05±0.09
0.25–0.30	0.27±0.14	0.54±0.13	0.12±0.13
0.30–0.35	0.42±0.14	0.41±0.15	0.11±0.11
0.35–0.40	0.30±0.16	0.38±0.18	0.33±0.16
0.40–0.50	0.40±0.19	0.54±0.19	0.03±0.13
0.50–0.60	0.43±0.18	0.41±0.18	0.17±0.16
0.60–0.70	0.52±0.14	0.14±0.15	0.35±0.13
0.70–0.80	0.83±0.14	0.00±0.10	0.19±0.12
0.80–1.00	0.82±0.11	0.01±0.08	0.21±0.10
1.00–1.20	0.83±0.12	0.05±0.09	0.05±0.09
1.20–1.60	0.63±0.13	0.08±0.10	0.22±0.11

TABLE X. $\rho_{11}+\rho_{1-1}$ and $\rho_{11}-\rho_{1-1}$ for $\pi^-p\to\rho^0 n$.

$\lvert t\rvert$ [(GeV/c)^2]	$\rho_{11}+\rho_{1-1}$	s channel $\rho_{11}-\rho_{1-1}$	t channel $\rho_{11}-\rho_{1-1}$
0.00–0.05	0.20±0.03	0.16±0.03	0.15±0.03
0.05–0.10	0.20±0.04	0.21±0.04	0.11±0.04
0.10–0.15	0.14±0.05	0.39±0.06	0.16±0.06
0.15–0.20	0.16±0.06	0.51±0.07	0.06±0.06
0.20–0.25	0.35±0.10	0.34±0.10	0.06±0.08
0.25–0.30	0.38±0.11	0.42±0.12	0.11±0.08
0.30–0.35	0.34±0.13	0.57±0.13	0.05±0.10
0.35–0.40	0.40±0.14	0.31±0.15	0.20±0.12
0.40–0.50	0.39±0.11	0.42±0.11	0.19±0.10
0.50–0.60	0.26±0.16	0.33±0.18	0.39±0.18
0.60–0.70	0.58±0.15	0.24±0.12	0.18±0.12
0.70–0.80	0.48±0.19	0.50±0.17	0.06±0.17
0.80–1.00	0.53±0.13	0.32±0.13	0.20±0.11
1.00–1.20	0.48±0.16	0.31±0.16	0.27±0.15
1.20–1.60	0.30±0.14	0.27±0.14	0.55±0.15

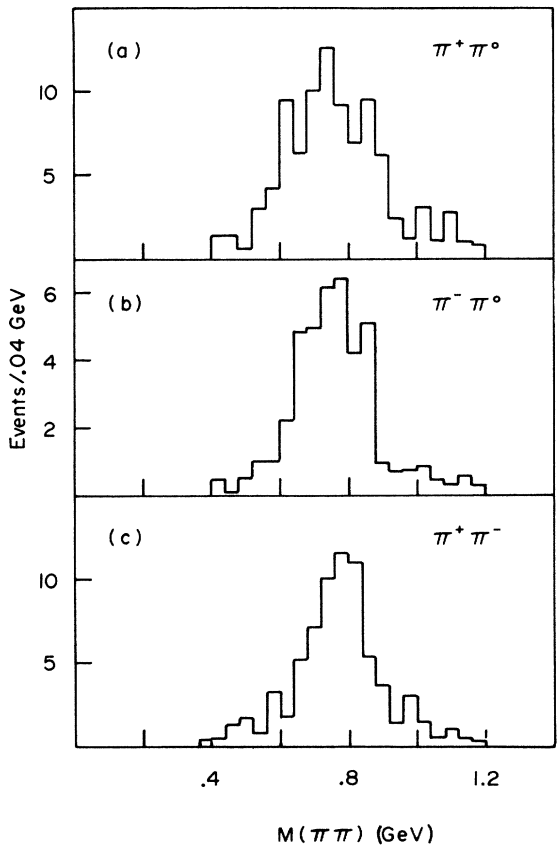

FIG. 10. Dipion mass distributions for events in the backward hemisphere selected as ρ mesons. (a) $\pi^+p\to p\rho^+$, (b) $\pi^-p\to p\rho^-$, (c) $\pi^-p\to n\rho^0$.

TABLE XI. Total cross section for backward production of ρ mesons.

	Events	σ (μb)
ρ^+	102	90±9
ρ^-	48	39±6
ρ^0	79	63±7

cylindrical Bessel function $J_1(R\sqrt{-t})$ with $R\sim 1.2$ F. This dip is predicted by both Dar[16] and Harari.[4] Dips appear in their models as zeros of $J_{\Delta\lambda}(R\sqrt{-t})$, which in turn is a consequence of strong central absorption in the impact-parameter plane.[7,16,17] $\Delta\lambda$ is the net helicity flip in the s channel. Different considerations show, in both strong[16] and dual absorption[4] models, that the $\Delta\lambda=1$ helicity-flip amplitude should dominate the ω-exchange amplitude.

Harari has formulated a dual absorptive model in which he hypothesizes that the imaginary part of the ω-exchange amplitude T should have the form[4,7]

$$\mathrm{Im}T = A^{1/2}e^{bt}J_1(R\sqrt{-t}). \tag{15}$$

Harari and Schwimmer[7] have proposed three classes of mutually incompatible models based upon the behavior of the parameters. For Class I and II models, the differential cross section for ω exchange takes on the simple form

$$\frac{d\sigma}{dt} = Ae^{2bt}J_1^2(R\sqrt{-t})[1+\tan^2(\tfrac{1}{2}\pi\alpha)], \tag{16}$$

where $\alpha(t)$ is the ω trajectory.

We have obtained a fit to this function for $|t|<1.6$ (GeV/c)^2 and compared our results with those from a similar fit at 6 and 16 GeV/c (Table XIV). Two trends are apparent: the constant value of R over a large range in s, and the increasing value of b between 6 and 16 GeV/c. This seems to favor Class I models over Class II models, but one would need additional points at higher energies in order to determine the class which best represents the data. The Class III model cannot describe the data with reasonable parameters (i.e., positive radius) and is therefore clearly not valid at these energies.

We have integrated the $I=0$ cross section for $|t|\leq 1.0$ (GeV/c)^2 and find a total cross section for $I=0$ exchange of 227±19 μb. For the $I=1$ amplitude we use relation (13) and the ρ^0 cross section to give $|I_1|^2=498\pm14$ μb. These cross sections, along with similarly derived cross sections from the higher momentum data previously quoted, are

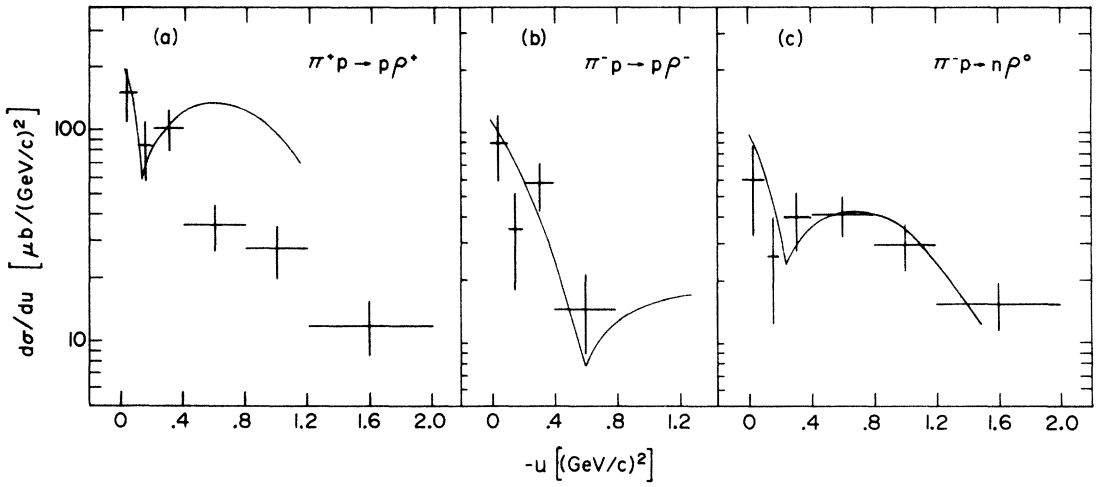

FIG. 11. The differential cross sections in the u channel for the three reactions (a) $\pi^+p \to \rho^+p$, (b) $\pi^-p \to \rho^-p$, and (c) $\pi^-p \to \rho^0n$. The curves represent the shape of the equivalent pion backward elastic and charge-exchange scattering with arbitrary normalization (see text).

shown in Fig. 14. An arbitrary systematic error of 10% has been folded into the error determined by integrating the quoted differential cross sections.

The trends in the data, however, appear to be significant even with unknown systematic differences of 10–20% between experiments. The $I=1$ cross section is dropping considerably faster than the $I=0$ cross section such that at 3.9 GeV/c their ratio is 2:1 while at 16 GeV/c they are almost equal. A fit of the form $\sigma \propto P_{\text{lab}}{}^{-n}$ has been carried out and gives values of $n=1.4\pm0.4$ for $I=0$ exchange and $n=2.3\pm0.1$ for $I=1$ exchange.

The hypothesis of pure ω exchange implies all natural-parity exchange. In Fig. 15 we show the matrix elements for the $I=0$ exchange calculated from the relation

TABLE XII. Differential cross sections for backward production of ρ mesons.

	$d\sigma/du$ [μb/(GeV/c^2)]		
$-u$ [(GeV/c)^2]	$\pi^+p \to \rho^+p$	$\pi^-p \to \rho^-p$	$\pi^-p \to \rho^0n$
−0.03–0.1	153±44	90±33	60±26
0.1–0.2	85±27	35±17	26±14
0.2–0.4	103±21	58±15	40±13
0.4–0.8	36±9	15±6	41±9
0.8–1.2	28±8	···	29±8
1.2–2.0	12±4	···	15±4

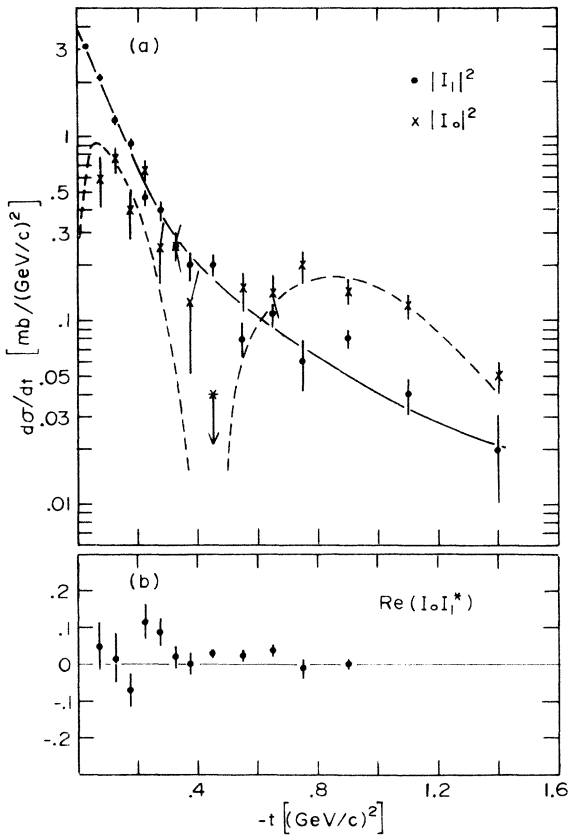

FIG. 12. (a) The square of the amplitude for the exchange of $I=0$ and $I=1$ particles in the t channel. The curve through the $I=1$ points is hand drawn to aid the eye. The curve through the $I=0$ points is from the fit to the Harari dual absorptive model (see text). (b) The real part of the interference between $I=0$ and $I=1$ exchange.

TABLE XIII. $d\sigma/dt$ for $I=0$ exchange in the reaction $\pi p \to \rho N$.

$\lvert t\rvert$ [(GeV/c)^2]	$d\sigma/dt$ [mb/(GeV/c)^2]
0.05–0.10	0.58 ± 0.20
0.10–0.15	0.76 ± 0.16
0.15–0.20	0.40 ± 0.13
0.20–0.25	0.65 ± 0.12
0.25–0.30	0.25 ± 0.09
0.30–0.35	0.26 ± 0.08
0.35–0.40	0.125 ± 0.067
0.40–0.50	0.005 ± 0.042
0.50–0.60	0.150 ± 0.035
0.60–0.70	0.135 ± 0.038
0.70–0.80	0.200 ± 0.038
0.80–1.00	0.140 ± 0.024
1.00–1.20	0.124 ± 0.021
1.20–1.60	0.054 ± 0.010

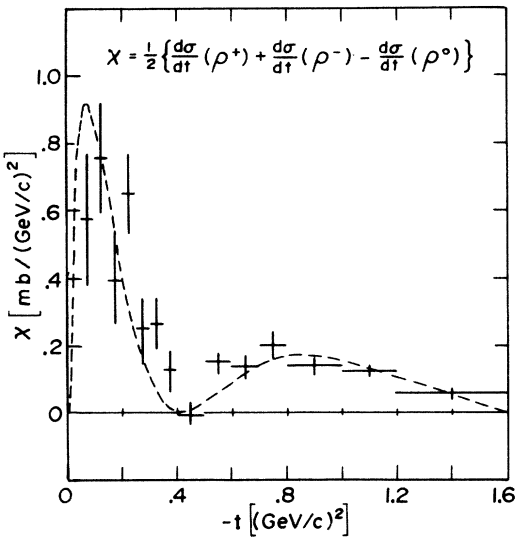

FIG. 13. The amplitude for $I=0$ exchange. The curve is a fit to the Harari dual absorptive model (see text).

$$\rho_{mn}(I=0) = \tfrac{1}{2}\left[\rho_{mn}\frac{d\sigma}{dt}(\rho^+) + \rho_{mn}\frac{d\sigma}{dt}(\rho^-) - \rho_{mn}\frac{d\sigma}{dt}(\rho^0)\right] \Big/ \left(\frac{d\sigma}{dt}\right)_{I=0}. \tag{17}$$

There are no points shown for $0.35 \leq |t| \leq 0.6$ (GeV/c)^2 because of the small value of the $I=0$ exchange cross section in that range. The result for $\rho_{11}+\rho_{1-1}$ is consistent with almost complete natural-parity exchange. The contribution isolated by the ρ^t_{00} matrix elements has the quantum numbers $I=0$, $G=-1$, and $P(-1)^J=-1$ which are not associated with any established particles. A large contribution from this exchange has been seen at 2.67 GeV/c (see Ref. 18) and a smaller contribution at 16.0 GeV/c.[6] In Fig. 16 we show the quantity

$$\chi_{00} = \tfrac{1}{2}\left[\rho^t_{00}\frac{d\sigma}{dt}(\rho^+) + \rho^t_{00}\frac{d\sigma}{dt}(\rho^-) - \rho^t_{00}\frac{d\sigma}{dt}(\rho^0)\right] \tag{18}$$

from our data, indicating a possible small $I_t=0$ nonflip unnatural-exchange contribution.

TABLE XIV. Values of parameters obtained fitting $d\sigma/dt\,|_{I=0}$ to Harari's absorption model at 3.9, 6, and 16 GeV/c.

Momentum [(GeV/c)]	s (GeV^2)	A [mb/(GeV/c)^2]	b [(GeV/c)$^{-2}$]	R (F)
3.9	8.2	2.07 ± 0.50	0.45 ± 0.15	1.20 ± 0.01
6	12.2	0.75 ± 0.14	0.47 ± 0.18	1.18 ± 0.02
16	31.0	0.46 ± 0.06	1.62 ± 0.25	1.08 ± 0.05

V. $I=1$ EXCHANGE

In Fig. 17 we show the product $\rho_{00}\,d\sigma/dt$ for the three charge states of the ρ meson in both the Gottfried-Jackson and helicity reference frames.

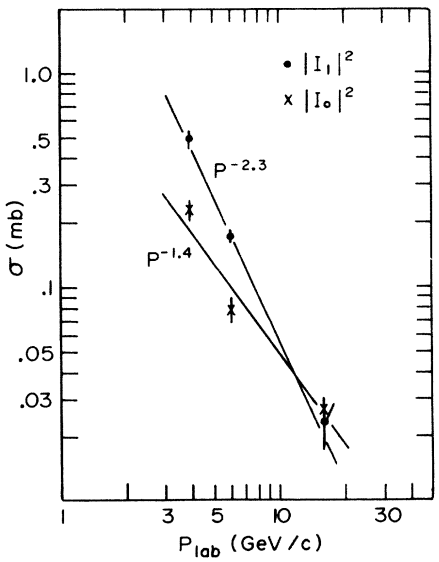

FIG. 14. The integrated cross section for $I=0$ and $I=1$ exchange to momentum transfers of 1.0 (GeV/c)^2. The points at 6 and 16 GeV/c are from Refs. 5 and 6, respectively. The line is a fit to the form $\sigma \propto P_{lab}^{-n}$.

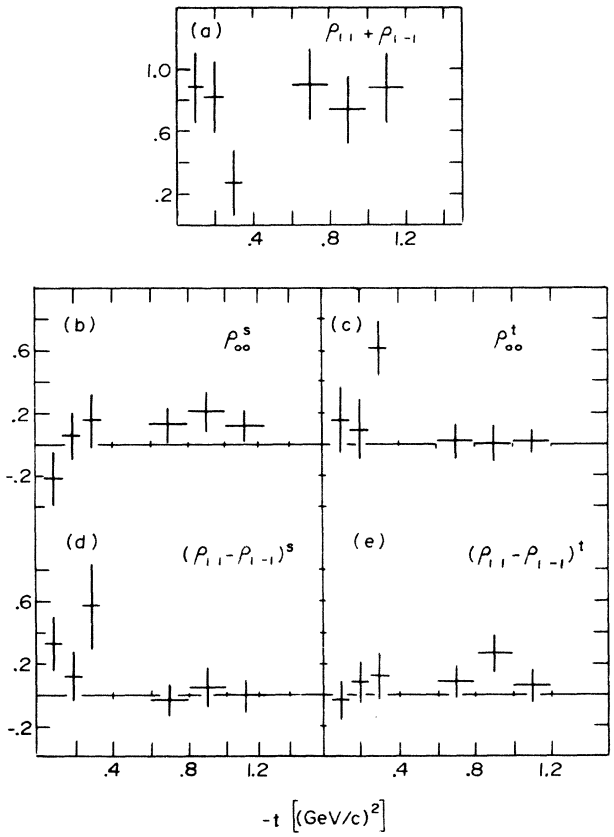

FIG. 15. The density matrix elements for $I = 0$ exchange. (a) $\rho_{11}+\rho_{1-1}$, (b) ρ_{00} (s channel), (c) ρ_{00} (t channel) (d) $\rho_{11}-\rho_{1-1}$ (s channel), (e) $\rho_{11}-\rho_{1-1}$ (t channel).

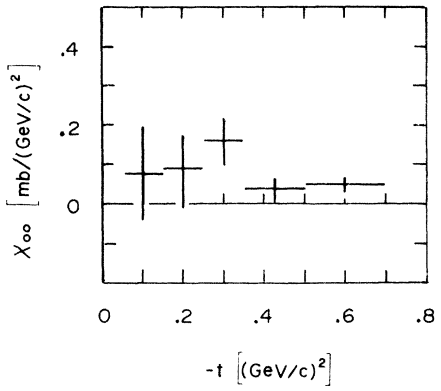

FIG. 16. Differential cross section for a t-channel exchange having the quantum numbers $I = 0$, $G = -1$, and $P(-1)^J = -1$.

This product, as previously mentioned, isolates the unnatural-parity exchange with no meson helicity flip. If the A_1 contribution is small, then this can be considered as pure π exchange. If we look in the helicity frame, then, as has been seen at other energies,[18,19] there appears to be a change in slope at $-t \sim 0.6$ (GeV/c)^2 (see Fig. 18). Unlike the case with ω exchange, where the dips in the cross section can be explained either by an absorptive model giving rise to a $J_1(R\sqrt{-t})$ behavior or a WSNZ point at the ω trajectory, only the absorptive models would predict structure at this point for the pion-exchange process.

VI. SUMMARY

In this paper we have presented our data on the nature of the exchange mechanisms present in the production of ρ mesons. The differential cross section has been obtained at all momentum transfers for the three reactions. In addition to the structure at small $|t|$, a dip is seen at $|t| \sim 3$ (GeV/c)^2 followed by a substantial backward peak for the production of all three mesons.

In the backward direction we have presented differential cross sections in the u channel for all three reactions. For the ρ^- and ρ^0 production, we find shapes which are very similar to the equivalent π^- backward elastic and charge-exchange scattering. There is a significant difference, however, between the ρ^+ backward production and the π^+ backward elastic scattering. Our ρ^+ data are similar to those found in experiments at 5.0 and 5.2 GeV/c although we have evidence for the presence of a dip at the WSNZ of the N_α trajectory which the other experiments do not.

The data in the forward direction can be explained to a high degree by a simple absorptive model, involving the exchange of the π and ω mesons. The contribution of the π meson decreases exponentially with momentum transfer, while the ω exchange shows a behavior like $J_1(R\sqrt{-t})$ with $R \sim 1.2$ F. The ω exchange therefore starts to dominate just past the first minimum at $-t = 0.45$ (GeV/c)^2, giving rise to the dip in the differential cross sections of ρ^+ and ρ^- and the sudden increase in natural-parity exchange at this point.

In the case of the ρ^0, where the ω cannot be exchanged, there is no dip and the dominant exchange at high momentum transfer is expected to be the A_2, which would also cause an increase in the natural-parity contribution. These observations can be more quantitatively tested through the use of an absorption model to predict the entire structure of $d\sigma/dt$ for each of the interactions and the t dependence of the matrix elements.

In the case of pure ω exchange there is good

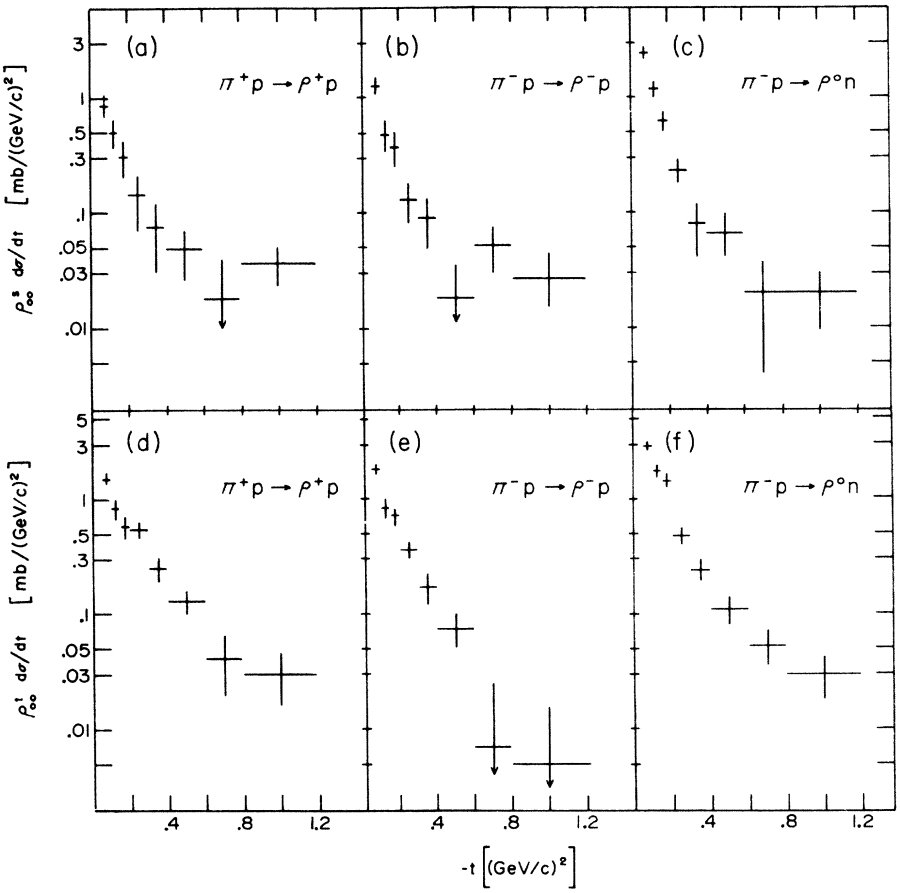

FIG. 17. $\rho_{00}d\sigma/dt$ in the Gottfried-Jackson frame for (a) $\pi^+p \to \rho^+p$, (b) $\pi^-p \to \rho^-p$, and (c) $\pi^-p \to \rho^0n$. The same quantity evaluated in the helicity frame for (d) $\pi^+p \to \rho^+p$, (e) $\pi^-p \to \rho^-p$, and (f) $\pi^-p \to \rho^0n$.

agreement with the Harari dual absorptive model for $|t|<1.6$ (GeV/c)^2 and the data seem to favor Class I of the models which he and Schwimmer have proposed. The total $I=0$ cross section for $|t|<1.0$ (GeV/c)^2 has been calculated and compared with the $I=1$ cross section for the same momentum transfer range. The $I=0$ cross section is seen to drop significantly more slowly than the $I=1$ cross section from 3.9 to 16.0 GeV/c.

There is also some evidence of an $I=0$ exchange with quantum numbers not associated with a known particle, but possibly associated with a Regge-cut exchange.

ACKNOWLEDGMENTS

We would like to express our gratitude to Dr. Gideon Berlad for many helpful discussions. We would like to thank the crew of the ANL 30 in. Bubble Chamber for their help during the exposure and to especially thank the scanning and measuring staff at MIT for their efforts.

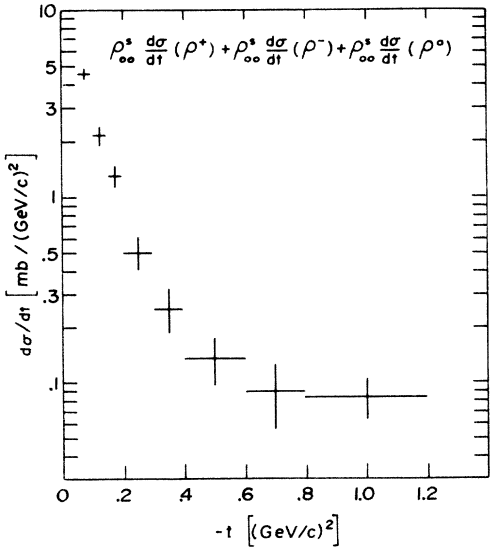

FIG. 18. The sum of $\rho^s_{00}\, d\sigma/dt$ for the three reactions $\pi^+p \to \rho^+p$, $\pi^-p \to \rho^-p$, and $\pi^-p \to \rho^0n$.

*This work is supported in part through funds provided by the U. S. Atomic Energy Commission under Contract No. AT(11-1) 3069.

†Present address: Weizmann Institute of Science, Israel.

‡On leave of absence from the Tel-Aviv University, Israel.

§Present address: Argonne National Laboratory, Argonne, Illinois.

[1]J. E. Brau, F. T. Dao, M. F. Hodous, I. A. Pless, and R. A. Singer, Phys. Rev. Lett. 27, 1481 (1971).

[2]F. T. Dao, M. F. Hodous, I. A. Pless, and R. A. Singer, DAS Programming Note 101, APC Group, MIT (unpublished).

[3]A. P. Contogouris, J. Tran Thanh Van, and H. J. Lubatti, Phys. Rev. Lett. 19, 1352 (1967).

[4]H. Harari, Phys. Rev. Lett. 26, 1400 (1971).

[5]D. J. Crennell *et al.*, Phys. Rev.Lett. 27, 1674 (1971); H. A. Gordon, K.-W. Lai, and J. M. Scarr, Phys. Rev. D 8, 779 (1973).

[6]J. Bartsch *et al.* (Aachen-Berlin-Bonn-CERN-Cracow-Heidelberg-Warsaw Collaboration), Nucl. Phys. B46, 46 (1972).

[7]H. Harari and A. Schwimmer, Phys. Rev. D 5, 2780 (1972).

[8]P. L. Bastien *et al.*, Phys. Rev. D 3, 2048 (1971); R. A. Singer, MIT thesis (unpublished).

[9]K. Gottfried and J. D. Jackson, Nuovo Cimento 33, 309 (1964).

[10]J. P. Adler, M. Capdeville, G. Cohen-Tannoudji, and Ph. Salin, Nuovo Cimento 56, 952 (1968).

[11]P. B. Johnson *et al.*, Phys. Rev. 176, 1651 (1968).

[12]Aachen-Berlin-Birmingham-Bonn-Hamburg-London-München Collaboration, Phys. Rev. 138, B897 (1965).

[13]J. Banaigs *et al.*, Nucl. Phys. B8, 31 (1968); R. C. Chase *et al.*, Phys. Rev. D 2, 2588 (1970); R. A. Sidwell *et al.*, *ibid.* 3, 1523 (1971). C. DeMarzo *et al.*, paper submitted to Second Aix-en-Provence International Conference on Elementary Particles, 1973 (unpublished).

[14]D. J. Schotanus *et al.* (Durham-Nijmegen-Paris-Torino Collaboration), Nucl. Phys. B22, 45 (1970).

[15]P. J. Carlson, P. Fleury, A. Lundby, S. Mukhin, and J. Myrheim, Phys. Lett. 33B, 502 (1970).

[16]A. Dar, Ann. Phys. (N.Y.) 69, 1 (1972).

[17]A. Dar, T. L. Watts, and V. F. Weisskopf, Nucl. Phys. B13, 477 (1969).

[18]W. Michael and G. Gidal, Phys. Rev. Lett. 28, 1475 (1972).

[19]J. M. Scarr and K.-W. Lai, Phys. Rev. Lett. 29, 310 (1972).

PHYSICAL REVIEW D VOLUME 10, NUMBER 5 1 SEPTEMBER 1974

Measurement of inclusive hadron electroproduction from hydrogen and deuterium*

J. T. Dakin,† G. J. Feldman, F. Martin, M. L. Perl, and W. T. Toner‡

Stanford Linear Accelerator Center, Stanford University, Stanford, California 94305

(Received 24 April 1974)

We report on the inclusive electroproduction of hadrons from nucleon targets. The incident electron beam energy is 19.5 GeV. We detect scattered electrons corresponding to exchanged virtual photons in the range $-0.25 > q^2 > -3.00$ (GeV/c)^2 and $12 < s < 30$ GeV^2. In coincidence we detect most hadrons which go in the forward (virtual photon) direction in the virtual-photon–nucleon c.m. system. The cross section for producing these hadrons is studied as a function of azimuthal angle, transverse momentum squared, and a longitudinal-momentum-related variable. Data are presented for proton, deuteron, and neutron targets, and are largely consistent with the data in real photoproduction ($q^2 = 0$). Notable differences are that in electroproduction the transverse momentum distributions are somewhat broader, and the forward hadrons are less charge- and isospin-symmetric. The data are generally consistent with expectations of parton models.

I. INTRODUCTION

We report here an experimental study of the final-state hadrons produced in inelastic electron-nucleon scattering. It has been observed that the cross section for electron-nucleon (e-N) scattering where only the final-state electron (e') is detected,

$$eN \to e' + \text{hadrons}, \tag{1}$$

exhibits a remarkable kinematic regularity which we will refer to as "leptonic scaling"[1] (to differentiate it from scaling in the hadronic final states, which we will discuss later). By investigating the single hadrons (h) ejected in coincidence with electrons,

$$eN \to e'h + \text{anything}, \tag{2}$$

we hope to gain insight into the physics underlying leptonic scaling. Brief accounts of this investigation have been reported earlier.[2] In addition to the inclusive reaction (2) considered here, we have also reported a study of the exclusive channels $ep \to ep\rho^0$ and $ep \to ep\varphi$.[3]

In the remainder of this section we will discuss